LBNL-49331

Numerical Simulation of Premixed Turbulent Methane Combustion

John B. Bell, Marcus S. Day and Joseph F. Grcar
Computing Sciences Directorate
Lawrence Berkeley National Laboratory
Berkeley, California 94720

This work was supported under the SciDAC Program by the Director, Office of Science, Office of Advanced Scientific Computing Research, Mathematical, Information, and Computational Sciences Division of the U.S. Department of Energy, contract No. DE-AC03-76SF00098.

Numerical Simulation of Premixed Turbulent Methane Combustion

Abstract

In this paper we study the behavior of a premixed turbulent methane flame in three dimensions using numerical simulation. The simulations are performed using an adaptive time-dependent low Mach number combustion algorithm based on a second-order projection formulation that conserves both species mass and total enthalpy. The species and enthalpy equations are treated using an operator-split approach that incorporates stiff integration techniques for modeling detailed chemical kinetics. The methodology also incorporates a mixture model for differential diffusion. For the simulations presented here, methane chemistry and transport are modeled using the DRM-19 (20-species, 84-reaction) mechanism derived from the GRIMech-1.2 mechanism along with its associated thermodynamics and transport databases. We consider a lean flame with equivalence ratio 0.8 for two different levels of turbulent intensity. For each case we examine the basic structure of the flame including turbulent flame speed and flame surface area. The results indicate that flame wrinkling is the dominant factor leading to the increased turbulent flame speed. Joint probability distributions are computed to establish a correlation between heat release and curvature. We also investigate the effect of turbulent flame interaction on the flame chemistry. We identify specific flame intermediates that are sensitive to turbulence and explore various correlations between these species and local flame curvature. We identify different mechanisms by which turbulence modulates the chemistry of the flame.

Introduction

Turbulence affects the process of combustion through a wide variety of mechanisms. Traditional approaches, based on asymptotic analysis, show that velocity-induced tangential strain at the flame surface can dramatically enhance or suppress combustion activity in the flame zone depending on Lewis number. These effects have been studied using results from steady flat-flame counterflow experiments (see [1–5]). As discussed in the review by Peters [6], this type of information can readily be incorporated into engineering models through the flamelet concept.

In recent years there have been a number of studies aimed at elucidating key mechanisms in premixed turbulent combustion using numerical simulation with detailed kinetics mechanisms. Many of these studies have focused on the interaction of a single vortical structure with a laminar premixed flame. Such studies typically consider either a planar vortex pair (for example, see [7–11]), or an axisymmetric toroidal vortex (for example, see [12–19]).

In two dimensions, Baum et al. [20] studied turbulent flame interactions for detailed hydrogen chemistry, and Haworth et al. [21] have examined the effect of inhomogeneous reactants for propane–air flames using detailed propane chemistry. More recently Tanahashi et al. [22] have performed direct numerical simulations of turbulent, premixed hydrogen flames in three dimensions with detailed hydrogen chemistry.

In this paper we investigate the behavior of premixed turbulent methane flames in three dimensions using numerical simulations with detailed chemistry. The computational setting is similar to the configuration used by Trouve and Poinsot [23] and by Zhang and Rutland [24] for single step chemistry and by Tanahashi et al. [22] for comprehensive hydrogen chemistry. We begin with a flat flame initialized using the laminar flame solution. A field of isoptropic decaying turbulence is superimposed on the incoming fuel stream; the flame deflects in response to the turbulent structures. We present two scenarios, representing different levels of turbulent intensity in the fuel stream. Analysis includes computation of an effective turbulent flame speed, flame surface area, and scatter plots to characterize the deviation of the flame from the laminar flame solution.

Numerical Model

Our computational approach uses a hierarchical adaptive mesh refinement (AMR) algorithm based on an approximate projection formulation for incompressible flow by Almgren et al. [25], subsequently extended to low Mach number combustion by Pember et al. [26]. The methodology was extended to model detailed kinetics and differential diffusion by Day and Bell [27]. The reader is referred to [27] for details of the model and its numerical implementation.

We consider a gaseous mixture, ignoring Soret and Dufour effects, body forces and radiative heat transfer, and assume a mixture model for species diffusion [28, 29]. The single-grid scheme that forms the basis for our adaptive algorithm combines a symmetric operator-split coupling of chemistry and diffusion processes with a projection method for incorporating the velocity divergence constraint arising from the low Mach number formulation. First, conservation equations are advanced in time for momentum, species density and enthalpy using a second-order Godunov scheme for advective terms and a time-centered Crank-Nicolson discretization for diffusion. Because the transport coefficients depend on both temperature and composition, we adopt a sequential, predictor-corrector scheme to guarantee second-order treatment of nonlinear diffusion effects. The chemistry is advanced using time-implicit backward differentiation methods in VODE [30]. The implicit diffusion and chemistry components of the algorithm are time-split symmetrically to ensure that the composite algorithm remains second-order. The velocity field resulting from the advection/diffusion/chemistry step is then decomposed using a density-weighted approximate

projection. The component satisfying the elliptic constraint updates the velocity field, and the remainder updates the perturbational pressure.

The extension of the above algorithm to AMR is based on a hierarchical refinement strategy using a system of overlaid grids with successively finer spacing in time and space. Fine grids are formed by uniformly dividing coarse cells in all three directions. Increasingly finer levels, each consisting of a union of rectangular grid patches, overlay coarser grid levels until the solution is adequately resolved. The fine grids are advanced in a subcycled fashion using a CFL-based time step appropriate to that level. Sychronization operations ensure appropriate coupling and conservation across refinement levels. An error estimation procedure identifies where refinement is needed and grid generation procedures dynamically create or remove rectangular fine grid patches as requirements change. The complete adaptive algorithm is second-order accurate in space and time, and discretely conserves species mass and enthalpy. The behavior of the method was thoroughly characterized in [27]. Implementation of this methodology for distributed memory parallel processors is discussed by Bell, et al. [31].

Results

Simulations are performed in a computational domain that measures 8×8×16mm. We use DRM-19 [32] (20-species, 84-reaction) for the chemistry mechanism, thermodynamics and transport databases. The flame is initialized with a steady laminer flat methane flame solution at equivalence ratio $\phi = 0.8$. The laminar flame thickness, $\delta_L = (T_b - T_u)/\max(|\nabla T|)$ is 53.3μm, and laminar flame speed, $S_L = 0.25$ m/s. Boundary conditions for the velocity fields on the 8×8mm inflow face are given as $\vec{u}(\vec{x},t) = 1.5\ S_L\hat{z} + \vec{u}\,'(\vec{x},t)$. The turbulent perturbations $\vec{u}\,'(\vec{x},t)$ are taken from an auxiliary calculation, and represent decaying isotropic turbulence in the fuel stream. The fluctuation field is generated with random phase in an 8×8×8mm triply-periodic box, and then allowed to evolve until realistic phases are established. The resulting field translates through the inflow boundary with a speed of $1.5S_L$ during the simulation—a value higher than S_L is used to keep the flame within the domain throughout the simulation. On initial startup, the perturbed velocity field is extended into the domain from the inflow boundary, and is damped to zero 1mm from the flame surface using a hyperbolic tangent profile.

The simulations are computed on a three-level adaptive grid hierarchy using a constant factor-of-two refinement between levels; the effective resolution is $\Delta x_{\mathit{eff}} = 62.5\mu$m. All refinement levels but the coarsest are localized dynamically to the region between the inflow boundary and the flame to ensure adequate resolution of both the flame and the incoming velocity fluctuations. To verify appropriate grid-independence, the analysis to follow was repeated using data from simulations a factor

of two finer ($\Delta x_{eff} = 31.25\mu$m); no substantive variations were observed. Typical simulations for $\Delta x_{eff} = 62.5\mu$m required approximately 750 hours wall clock time using 64-96 processors of an IBM SP3.

For the domain considered here, the Reynolds number, $Re_t = u'\ell_t/\nu \sim 100$, based on the unburned fuel and turbulent fluctuations at the inflow boundary. The turbulent fluctuations decay as they propagate toward the flame. Using two different initial altitudes for the flame we investigated two different turbulent intensities within the same problem configuration. In the first case, the flame is initialized at z=8mm (based on the peak value of heat release), and the flame encounters an upstream turbulence intensity of approximately .45m/s ($\approx 1.7S_L$). In the second case, the flame is initialized at z=4mm, where the upstream turbulence intensity is approximately 1.1m/s ($\approx 4.3S_L$). We will refer to these cases as the weak and strong cases, respectively.

In Fig. 1, we show volume rendered images of the heat release that represent the overall flame surface. As expected, stronger turbulence leads to increased wrinkling of the flame. To quantify this notion, we observe that the peak heat release for this flame correlates with a temperature of approximately 1500K. We then approximate the flame surface area by the area of the $T = 1500$K isosurface. For the weak and strong cases we obtain $1.23A_L$ and $1.64A_L$, respectively, where A_L is the flame surface area for the corresponding flat laminar flame.

We can compute the net consumption rate of CH_4 integrated over the computational domain. The fuel consumption rate, suitably scaled, gives the turbulent flame speed. For the weak and strong cases, we obtain $S_T = 1.35\ S_L$ and $S_T = 1.85\ S_L$, respectively. Comparing these speeds to the increases in flame area we see that the dominant factor in enhancing the flame speed is the increase in flame surface area associated with the wrinkling of the flame. However, since the flame speed increases faster than the surface area, it is clear that the turbulence is actually modifying the flame chemistry. The observed trend is consistent with earlier 2D studies [33] based on single-step Arrhenius chemistry. The present fuel-lean cases correspond to $Le < 1$, where Le is based on the deficient reactant. There is, however, substantial variation in flame intensity across the flame surface. To quantify this variation, we compute the joint probability distribution function of heat release and mean curvature, κ, of the flame surface with the convention that positive curvature means the flame is concave toward the burned products, $\kappa = -\nabla \cdot \hat{n}$, where $\hat{n}$, the flame normal, is taken along the temperature gradient (the reader is cautioned that some authors use the alternate sign convention for κ). In Fig. 2 we show the joint PDF's for the weak and strong turbulence cases. The two PDF's are quite similar, with the stronger turbulence showing a greater variation in curvature. Both images show a strong correlation between heat release and curvature. Tanahasi et al. [22] found a similar result for hydrogen flames.

As a first step toward analyzing the local effect of turbulence on chemistry, we compute scatter plots of species mole fraction versus temperature and compare the

result to the laminar flame solution parameterized by temperature. For the combination of turbulent intensity, integral scale and equivalence ratio considered here, most of the species mole fractions remain tightly clustered around the laminar flame solution. Fig. 3a, which shows the mole fraction of HCO versus T, is typical of most other species. In Fig. 3b, we show a scatter plot of the HCO mole fraction versus total heat release, Q. The correlation between peak heat release and HCO, in both the laminar and turbulent cases, indicates that HCO is a good flame marker for these flames as was oberved by Najm et al. [8] for vortex flame interaction.

There are four species, HO_2, H_2, CH_3O and C_2H_4, that show substantial variation in mole fraction compared to the laminar flame solution. Scatter plots for these four species are presented in Fig. 4. For each species the variability increases with increasing turbulent intensity. We note also that the variability arises primarily on the cold side of the flame. Above 1500K the mole fractions of these species cluster around the laminar flame solution.

In Fig. 5 we show typical vertical slices of the CH_3O and C_2H_4 mole fractions from the strong turbulence case. For strong negative curvature we see an abundance of CH_3O and an absence of C_2H_4 with the opposite occuring in regions of strong negative curvature. This point is further illustrated by the joint PDF's of the CH_3O and C_2H_4 mole fractions versus κ shown in Fig. 6. CH_3O, which is enhanced in regions of negative curvature, is created primarily from reaction of CH_3 and HO_2. Where the curvature is negative, we observe enhanced CH_3 and HO_2 concentrations, as well as elevated temperatures due to decreased thermal gradients. These factors lead to increases in the CH_3O production by as much as a factor of three. On the other hand, the velocity normal to the flame is enhanced through this region by as much as 50% from the laminar case, decreasing the residence time of the CH_3O molecules. Competition between these effects leads to an overal factor-of-two increase in CH_3O concentration. Where the curvature is positive, production of CH_3O is nearly eliminated, and the corresponding mole fraction is significantly decreased.

The mechanism for enhanced C_2H_4 in regions of positive curvature is quite different. In this case, the positive curvature tends to broaden the production zone slightly towards the upstream direction, but to otherwise have very little effect on the chemical rates for C_2H_4. However, the fluid velocity normal to the flame surface is reduced in the positively-curved regions to as little as 25% of its flat-flame value. Consequently, for equivalent production rates, the longer residence times resulting from the lower velocity tends to enhance the integrated production of C_2H_4 molecules over the flat flame values. In regions of negative curvature, chemical production rates for C_2H_4 are similarly unaffected. Since the velocity increases in regions of negative curvature are of the order of 50%, a less dramatic, oppositely signed effect is observed. The behavior of CH_3O and C_2H_4 illustrate two distinct mechanisms by which turbulence modulates detailed flame chemistry.

Conclusions

In this paper we have used numerical simulations with detailed chemistry to study the behavior of turbulent, premixed methane combustion in three space dimensions. Two cases, corresponding to varying levels of turbulent intensity, show increased flame area and enhancements of the laminar flame speed by 35% and 85%. The flame speed increases somewhat faster than flame surface area, consistent with earlier single-step 2D studies with $Le < 1$. The basic flame structure exhibits a correlation between heat release and curvature. We also show similar correlations between some of the flame intermediaries and curvature illustrating the local variability of the chemistry. A more detailed analysis reveals two distinct scenarios leading to curvature dependence. Production of some of the chemical species correlates strongly with flame curvature, as does the local velocity normal to the flame. These two effects shift the balance that determines the prevailing species concentrations.

Future work will include include a broader range of turbulence scales, more detailed methane mechanisms, and a range of configurations relevant to lean premixed combustion experiments, such as turbulent jets and swirl burners.

References

[1] F. Egolfopoulos. Dynamics and structure of unsteady, strained, laminar premixed flames. *Proc. Combust. Inst.*, 25:1365–1373, 1994.

[2] R. J. Kee, J. A. Miller, G. H. Evans, and G. Dixon-Lewis. A computational model of the structure and extinction of strained, opposed flow premixed methane-air flames. *Proc. Combust. Inst.*, 22:1479–1494, 1988.

[3] C. K. Law. Dynamics of stretched flames. *Proc. Combust. Inst.*, 22:1381–1402, 1988.

[4] C. Petrov and A. Ghoniem. The transient response of strained laminar-premixed flames. *Combust. Flame*, 102:401–417, 1995.

[5] B. Rogg. Response and flamelet structure of stretched premixed methane-air flames. *Combust. Flame*, 73:45–46, 1988.

[6] N. Peters. Laminar flamelet concepts in turbulent combustion. *Proc. Combust. Inst.*, 21:1231–1250, 1986.

[7] H. N. Najm and P. S. Wyckoff. Premixed flame response to unsteady strain rate and curvature. *Combust. Flame*, 110(1-2):92–112, 1997.

[8] H. N. Najm, O. M.. Knio, P. P. Paul, and P. S. Wyckoff. A study of flame observables in premixed methane-air flames. *Combust. Sci. Technol.*, 140:369–403, 1998.

[9] H. N. Najm, P. P. Paul, C. J. Mueller, and P. S. Wyckoff. On the adequacy of certain experimental observables as measurements of flame burning rate. *Combust. Flame*, 113(3):312–332, 1998.

[10] T. Mantel and J.-M. Samaniego. Fundamental mechanisms in premixed turbulent flame propagation via flame-vortex interactions Part II: Numerical simulation. *Combust. Flame*, 118:557–582, 1999.

[11] J. B. Bell, N. J. Brown, M. S. Day, M. Frenklach, J. F. Grcar, and S. R. Tonse. The dependence of chemistry on the inlet equivalence ratio in vortex-flame interactions. *Proc. Combust. Inst.*, 28:1933–1939, 2000.

[12] J. F. Driscoll, D. J. Sutkus, W. L. Roberts, M. E. Post, and L. P. Goss. The strain exerted by a vortex on a flame - determined from velocity field images. *Combust. Sci. Technol.*, 96:213–229, 1996.

[13] C. J. Mueller, J. F. Driscoll, D. L. Reuss, and M. C. Drake. Effect of unsteady stretch on the strength of a freely-propagating flame wrinkled by a vortex. *Proc. Combust. Inst.*, 26:347–355, 1996.

[14] C. J. Mueller, J. F. Driscoll, D. L. Reuss, M. C. Drake, and Martin E. Rosalik. Vorticity generation and attenuation as vortices convect through a premixed flame. *Combust. Flame*, 112(3):342–358, 1998.

[15] C. J. Mueller, J. F. Driscoll, D. J. Sutkus, W. L. Roberts, M. C. Drake, and M. D. Smooke. Effects of unsteady stretch rate on OH chemistry during a flame-vortex interaction: To assess flamelet models. *Combust. Flame*, 100:323–331, 1995.

[16] W. L. Roberts and J. F. Driscoll. A laminar vortex interacting with a premixed flame: Measured formation of pockets of reactants. *Combust. Flame*, 87:245–256, 1991.

[17] W. L. Roberts, J. F. Driscoll, M. C. Drake, and L. P. Goss. Images of the quenching of a flame by a vortex — To quantify regimes of turbulent combustion. *Combust. Flame*, 98:58–69, 1993.

[18] W. L. Roberts, J. F. Driscoll, M. C. Drake, and J. W. Ratcliffe. OH fluorescence images of the quenching of a premixed flame during an interaction with a vortex. *Proc. Combust. Inst.*, 24:169, 1992.

[19] J. C. Rolon, F. Aguerre, and S. Candel. Experiments on the interaction between a vortex and a strained diffusion flame. *Combust. Flame*, 100(3):422–429, 1995.

[20] M. Baum, T. J. Poinsot, D. C. Haworth, and N. Darabiha. Direct numerical simulation of $H_2/O_2/N_2$ flames with complex chemistry in two-dimensional turbulent flows. *J. Fluid Mech.*, 281:1–32, 1994.

[21] D. C. Haworth, R. J. Blint, B. Cuenot, and T. J. Poinsot. Numerical simulation of turbulent propane-air combustion with nonhomogeneous reactants. *Combust. Flame*, 121:395–417, 2000.

[22] M. Tanahasi, M. Fujimura, and T. Miyauchi. Coherent fine scale eddies in turbulent premixed flames. *Proc. Combust. Inst.*, 28:529–535, 1998.

[23] A. Trouve and T. Poinsot. The evolution equation for the flame surface density in turbulent premixed combustion. *J. Fluid Mech.*, 278:1–31, 1994.

[24] S. Zhang and C. J. Rutland. Premixed flame effects on turbulence and pressure-related terms. *Combust. Flame*, 102:447–461, 1995.

[25] A. S. Almgren, J. B. Bell, P. Colella, L. H. Howell, and M. Welcome. A conservative adaptive projection method for the variable density incompressible Navier-Stokes equations. *J. Comput. Phys.*, 142:1–46, 1998.

[26] R. B. Pember, L. H. Howell, J. B. Bell, P. Colella, W. Y. Crutchfield, W. A. Fiveland, and J. P. Jessee. An adaptive projection method for unsteady, low-Mach number combustion. *Comb. Sci. Technol.*, 140:123–168, 1998.

[27] M. S. Day and J. B. Bell. Numerical simulation of laminar reacting flows with complex chemistry. *Combust. Theory Modelling*, 4(4):535–556, 2000.

[28] R. J. Kee, G. Dixon-Lewis, J. Warnatz, M. E. Coltrin, and J. A. Miler. A FORTRAN computer code package for the evaluation of gas-phase multicomponent transport properties. Sandia Technical Report SAND86-8246, Sandia National Laboratories, 1986.

[29] J. Warnatz. Influence of transport models and boundary conditions on flame structure. In N. Peters and J. Warnatz, editors, *Numerical methods in flame propagation*. Friedr. Viewweg and Sohn, Wiesbaden, 1982.

[30] P. N. Brown, G. D. Byrne, and A. C. Hindmarsh. VODE: A variable coefficient ode solver. *SIAM J. Sci. Stat. Comput.*, 10:1038–1051, 1989.

[31] J. B. Bell, M. S. Day, A. S. Almgren, M. J. Lijewski, and C. A. Rendleman. A parallel adaptive projection method for low mach number flows. In M. J. Baines, editor, *Numerical Methods for Fluid Dynamics VII*, pages 207–213, Oxford and Reading Universities, March 2001. ICFD. *also to appear in Int. J. Num. Meth. Fluids*.

[32] A. Kazakov and M. Frenklach. Reduced reaction sets based on GRI-Mech 1.2. `http://www.me.berkeley.edu/drm/`.

[33] D. C. Haworth and T. J. Poinsot. Numerical simulations of Lewis number effects in turbulent premixed flames. *J. Fluid Mech.*, 244:405–436, 1992.

(a) 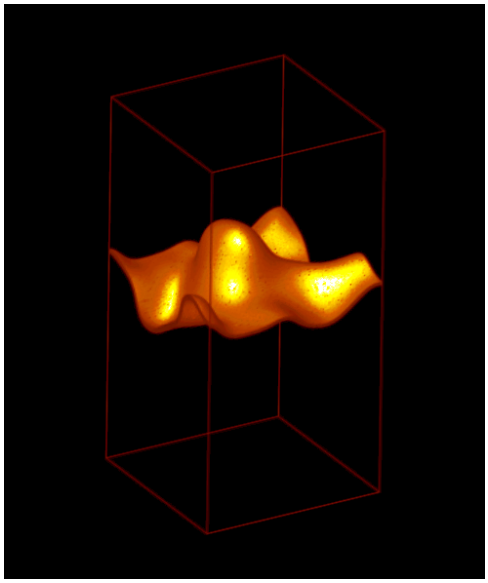 (b) 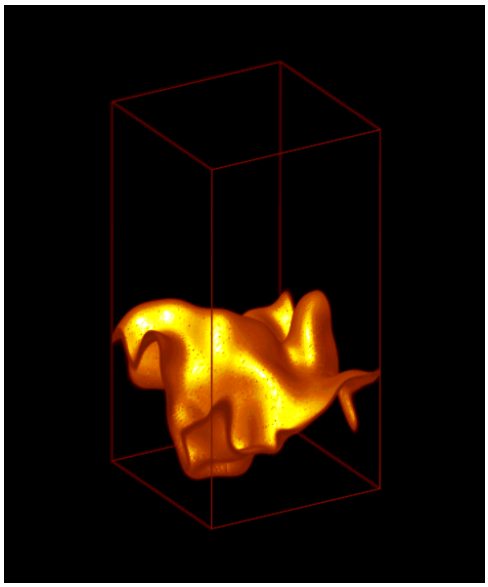

Figure 1 : *Volume rendered image showing surface of maximum heat release for the weak (a) and strong (b) turbulence cases.*

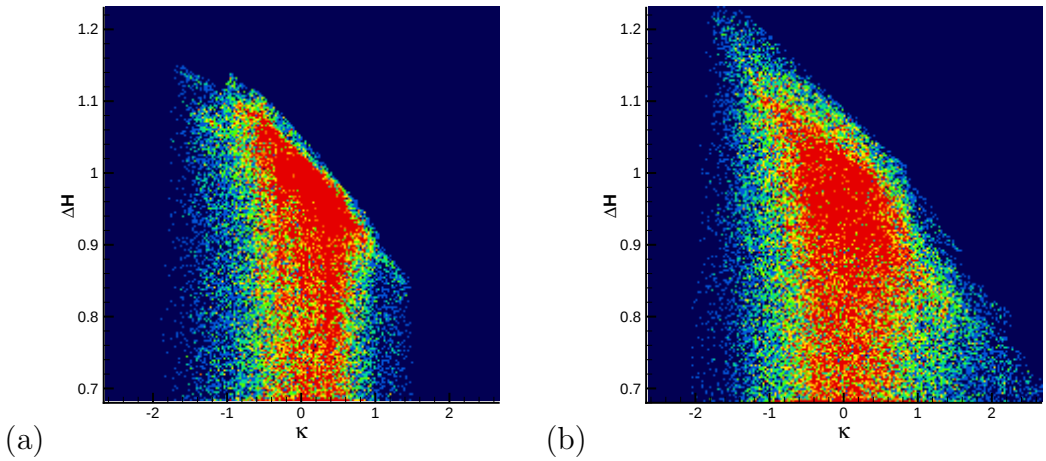

Figure 2 : *Joint probability distribution of heat release and mean curvature. The color scale is a standard rainbow palette with dark blue corresponding to zero probability and red indicating probabilities greater than* 1.4×10^{-6}. *The heat release is scaled by the peak value,* ΔH_L, *attained by the initial flat laminar flame,* $\Delta H_L = 2.2 \times 10^9\ J/m^3 s$. *The curvature is scaled by the inverse of the flat flame thickness,* δ_L. *Here, (a) is the weak turbulence case and (b) is the strong case.*

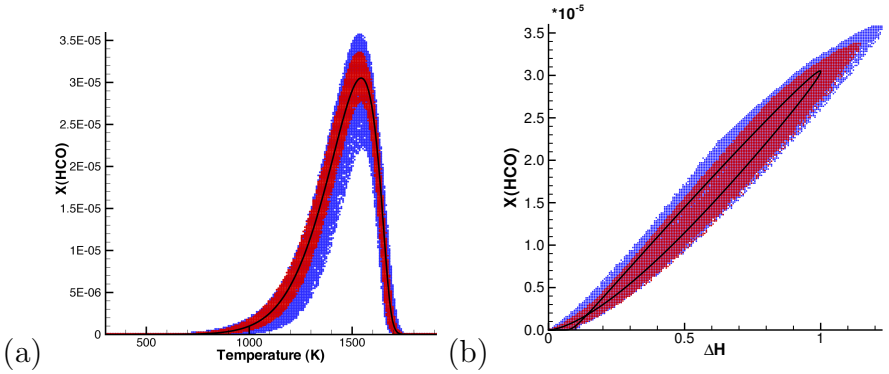

Figure 3 : *(a) Scatter plot of the HCO mole fraction vs. T. (b) Scatter plot of the HCO mole fraction vs. heat release,* ΔH. *The heat release is scaled by the peak value,* ΔH_L, *attained by the initial flat laminar flame,* $\Delta H_L = 2.2 \times 10^9\ J/m^3 s$. *The blue dots are for strong turbulence and the overlayed red dots are for weak turbulence. The black lines indicate the laminar flame solution.*

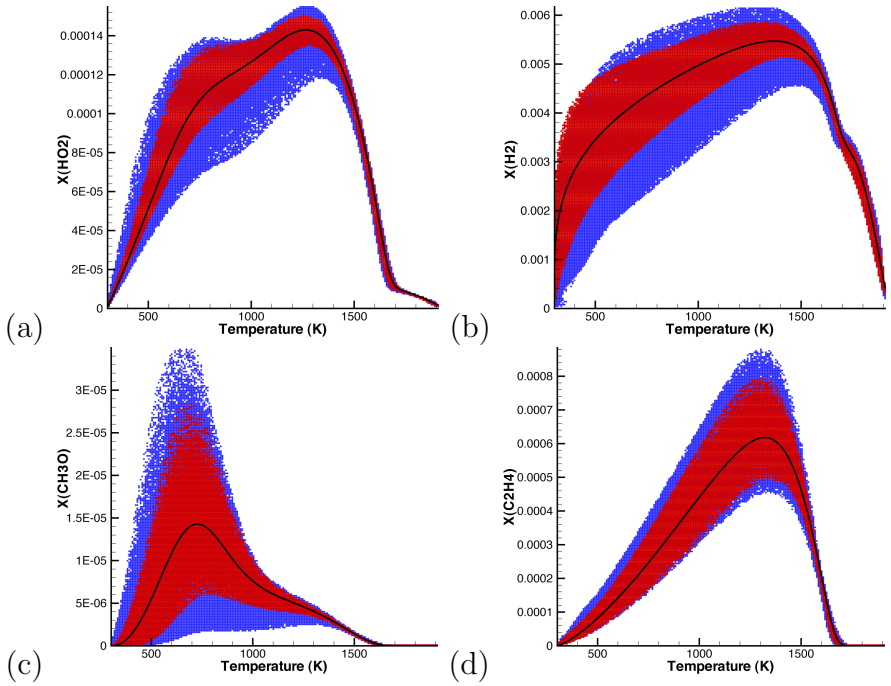

Figure 4 : *Scatter plots of mole fraction of (a) HO_2, (b) H_2, (c) CH_3O, and (d) C_2H_4 versus T. Turbulence-induced variations from the laminar solution appear to be localized to the cold regions. The remaining 16 species showed no appreciable variation from the laminar solution. The blue dots are for strong turbulence and the overlayed red dots are for weak turbulence. The black lines indicate the laminar flame solution.*

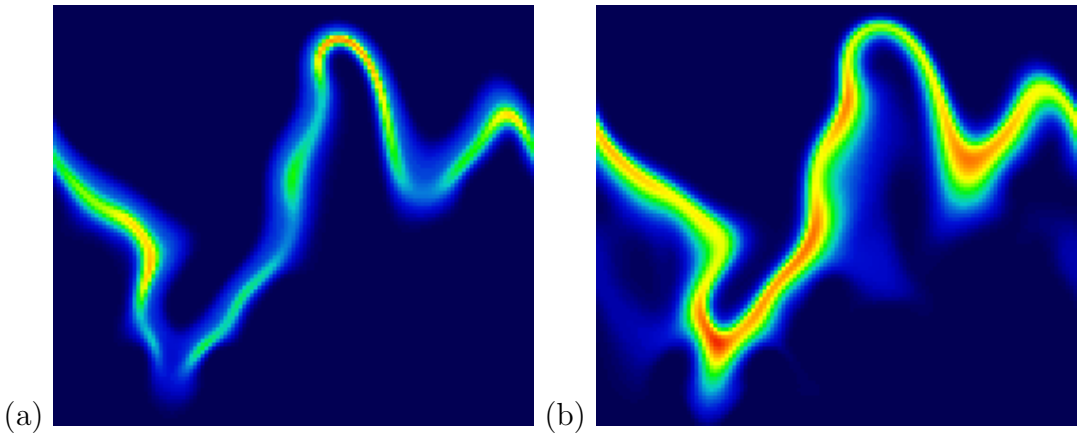

Figure 5 : *Vertical slices from the strong turbulence case showing mole fractions of (a) CH_3O and (b) C_2H_4 using a rainbow color palette. In regions of negative curvature, CH_3O is enhanced and C_2H_4 is suppressed. The converse is true in regions of positive curvature.*

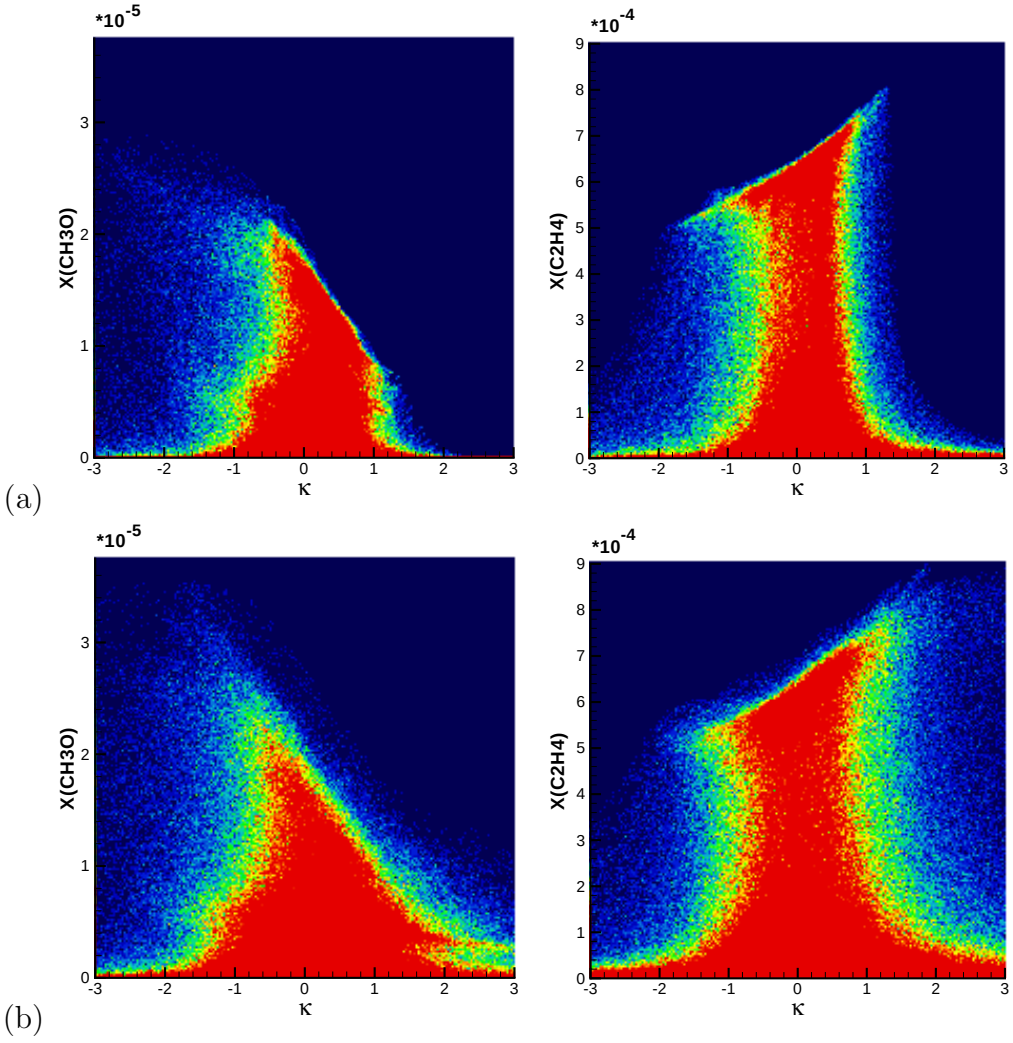

Figure 6 : *Joint probability distributions for CH_3O and C_2H_4 vs. κ for both the (a) weak and (b) strong turbulence cases. Here, the values are scaled so that red corresponds to probabilities greater than* 5×10^{-6}.